International Journal of Precision Engineering and Manufacturing (2020) 21:1597–1613
https://doi.org/10.1007/s12541-020-00366-0

Online ISSN 2005-4602
Print ISSN 2234-7593

REGULAR PAPER

Minimization of Surface Roughness and Machining Deformation in Milling of Al Alloy Thin-Walled Parts

De-Jun Cheng[1] · Feng Xu[1] · Sheng-Hao Xu[1] · Chun-Yan Zhang[1] · Sheng-Wen Zhang[1] · Su-Jin Kim[2]

Received: 26 December 2019 / Revised: 27 April 2020 / Accepted: 21 May 2020 / Published online: 17 June 2020
© Korean Society for Precision Engineering 2020

Abstract
This study focused on investigating the surface roughness in the feed direction (R_a-*Fd*), surface roughness in the transverse direction (R_a-*Td*), and thin-walled parts deformation (TWD) during milling of Al alloy 5083. The response surface method (RSM) was used to conduct experiments and establish the models of R_a-*Fd*, R_a-*Td*, and TWD under various cutting parameters. The significance of cutting parameters on R_a-*Fd*, R_a-*Td*, and TWD was analyzed by analysis of variance. It was observed that the R_a-*Fd* and R_a-*Td* are mainly influenced by the spindle speed, depth of cut, transverse size and feed rate, while the TWD is mainly influenced by the depth of cut. A comparison of RSM-optimum function and artificial bee colony (ABC) algorithm optimum programming was conducted to obtain the best cutting conditions leading to minimum R_a-*Fd*, R_a-*Td* and TWD simultaneously. From the presented results, ABC algorithm was able to obtain the better cutting strategy. Finally, the performance of the proposed cutting strategy was verified by confirmation experiments.

Keywords Surface roughness · Thin-walled parts deformation · RSM · ANOVA · ABC algorithm

1 Introduction

Al alloy has the characteristics of low density, high strength, corrosion resistance, good formability and low cost. Thus, it is widely used in aerospace, automotive, shipbuilding, plastic molding, and electronics applications [1–5]. In general, thin-walled parts refer to lightweight structural parts composed of various thin plates and stiffeners, and the wall thickness is less than 2.5 mm or the ratio between wall thickness and outline size is less than 1:10 [6]. During machining of thin-walled parts, the thin sections elastically deform occurs due to the low stiffness [7]. This is a common problem in the machining of Al alloy thin-wall components. Surface roughness is also one of the significant indexes to measure the performance of thin-walled parts. The value of surface roughness directly affects the wear resistance, fatigue strength, corrosion resistance, lubrication and friction of thin-walled parts [8, 9]. Thus, machining of Al alloy thin-wall components essentially requires precise setting of machining parameters to obtain the desired process performance i.e. dimensional accuracy and superior quality surface finish [6].

Recently, some researchers studied on the prediction of surface roughness, thin-walled parts deformation, and optimization of the cutting parameters. Wang et al. [10] carried out cutting experiments on AlMn1Cu, and established a surface roughness prediction model based on cutting parameters through partial least squares regression. Hao et al. [3] introduced the tool wear model and the tool forced deformation model into the basic roughness prediction model to improve the roughness model, which is a comprehensive prediction model for the surface roughness of curved thin-walled parts. Khanghah et al. [11] established an empirical model of stainless steel 316 using the RSM and ANOVA. Then, it is associated with simulated annealing to obtain the minimum optimal combination of parameters for the burr characteristics in both up-milling and down-milling processes. Zeng et al. [12] proposed a forward milling process parameters optimization method based on the real-coded self-adaptive genetic algorithm and Grey relational analysis, and validated the effectiveness of the model through additional experiments. Vipindas et al. [13] investigated the influences of surface roughness and top burr on the milling of Ti–6Al–4V

✉ Sheng-Wen Zhang
swzhang2003@163.com

[1] School of Mechanical Engineering, Jiangsu University of Science and Technology, Zhenjiang 212003, China

[2] School of Mechanical Engineering, Gyeongsang National University, Jinju 52828, Korea

with 0.5 mm and 1 mm cemented carbide tools by ANOVA, and reported the significant factors. Neelesh et al. [14] proposed a surface roughness model of high-speed machining Ti–6Al–4V by ANOVA with stepwise backward elimination method, and obtained the optimal combination of process parameters with minimum surface roughness.

In addition, Taguchi method was also applied widely to analyze the significance of cutting parameters on surface roughness during milling and optimized the process parameters [15–17]. Mahesh et al. [18] proposed a second-order mathematical models of surface roughness using RSM. Then, the genetic algorithm (GA) was applied to obtain the optimum cutting parameters via MATLAB programming. Kan and Lmalghan et al. [19, 20] constructed a comprehensive prediction model of surface roughness integrated into particle swarm optimization (PSO) algorithm. Dikshit et al. [4] studied the effect of cutting parameters on surface roughness in high-speed milling of Al2014–T6, and established an empirical mathematical model for surface roughness. It reported that the most significant is cutting speed followed by feed rate. Ying et al. [21] established the surface roughness model through BP artificial neural network algorithm with considering material removal rate, and optimized the processing parameters. Sheng et al. [22] established a regression model of cutting force and surface roughness through experimental results, and obtained the optimal milling parameters for thin-walled parts via non-dominated sorting genetic algorithm (NSGA-II) to. Karkalos et al. [23] developed an ANN model for predicting the surface roughness of titanium alloy and indicated that the ANN model was able to predict the surface roughness with a mean error of 0.97%. Gao et al. [24] proposed a deformation control strategy by modifying tool location point for deformation of thin-walled curved surface parts. Wang et al. [25] applied the particle swarm algorithm to establish the machining residual stresses model, and validated the prediction model by two cases. Qiong et al. [26] applied the Finite difference method (FDM) to predict the aerospace thin-walled plates and compared with the finite element method (FEM). Yue et al. [27] proposed a method to calculate the surface error with considering the chip thickness and coupling force. Song et al. [28] applied thin palate theory in developing a time-space discretization method for milling of thin-walled parts stability. The effect of residual stress on the thin-walled parts deformation was investigated with considering the heat treatment process, cutting parameters and machining process [29–33]. Sepp et al. [34] proposed a milling error prediction method for the outer surface of thin-walled parts based on the selection range of tools and process parameters. Wang et al. [35] proposed a methodology of 3D machining allowance modeling and analyzed the machining deformation of aerospace thin-walled parts.

Although many studies have been done in optimization of milling parameters, fewer surveys are performed with consideration of machining deformation and surface quality simultaneously in milling thin-walled plates. Moreover, most of the previous papers are available for identifying the optimal machining parameters by incorporating the soft computing techniques Taguchi method, GA, BP, PSO, NSGA-II and ANN. Therefore, this study explores the feasibility for multi-objective optimization with the RSM-ABC method, which is employed to optimize the R_a-*Fd*, R_a-*Td* and *TWD* simultaneously in Al alloy thin-walled parts machining process. In this paper, experiments were conducted to investigate the influence of cutting parameters on surface roughness and machining deformation simultaneously. Especially for the spindle speed and feed rate with a wider range were selected to increase the cutting efficiency. The models of R_a-*Fd*, R_a-*Td*, and *TWD* were developed using RSM with considering spindle speed (*S*), feed rate (*f*), transverse size (*ts*), and depth of cut (*doc*). The significance of cutting parameters on surface roughness and machining deformation was analyzed by ANOVA. A comparison of RSM-optimum function and ABC algorithm optimum programming was performed to obtain the best cutting conditions leading to minimum R_a-*Fd*, R_a-*Td* and *TWD* simultaneously. Finally, the optimization cutting parameters was implemented through experiments, which validates the feasibility of the proposed cutting strategy.

2 Experimental Procedure

The high-speed milling operations were conducted on Quick Jet AV1612 machining center that is equipped with HEIDENHAIN CNC system for precise control of machining process, which has a maximum spindle speed of 20,000 rpm and feed rate of 25 m/min. The workpiece selected for the experiment was Al alloy 5083 that has a rectangle block shape of 140 mm × 70 mm × 5 mm. The workpiece was mounted on a special fixture by applying 6 bolts further clamped on the bed of machine tool. The composition of workpiece material is given by Table 1.

In this test, a three-edge carbide flat end mill was employed which has a diameter of 12 mm, a helix angle of 40°, a radial rake angle of 13°, and a radial relief angle of

Table 1 Chemical composition of workpiece Al alloy 5083

Elements	Al	Cr	Cu	Mg	Mn	Si	Ti	Zn
Wt (%)	Balance	0.2	0.1	4.5	0.6	0.4	0.15	0.25

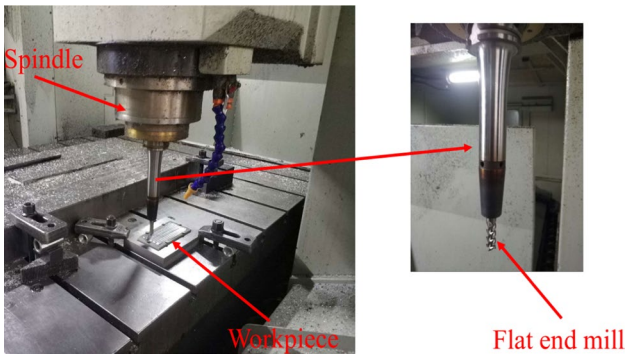

Fig. 1 Experimental setup

Table 2 Cutting parameters and their ranges

Cutting parameters	Symbols	Units	Ranges	
			Min	Max
Spindle speed	*S*	rpm	9000	15,000
Feed rate	*F*	mm/min	3600	9000
Depth of cut	*doc*	mm	0.1	0.3
Transverse size	*ts*	mm	3	7

14°. The cutting tool path was programmed by using *NX* 10 software, and the follow periphery tool path strategy was employed to guarantee the machined surface quality. Figure 1 shows the schematic of the setup milling experiment. The chosen cutting parameters and their ranges are shown in Table 2.

In this study, following the investigation method of surface roughness proposed from Refs. [36–38]. The surface roughness is investigated along two directions: feed direction and transverse direction. According to scallop height model [36, 37], the values of feed rate and transverse size are the important control factors in the calculation of the surface residual height. In addition, surface roughness along the feed direction and along the transverse direction has different spatial patterns [39]. Thereby, the surface roughness evaluated in R_a pattern was investigated in two directions can achieve optimum surface quality of the milling process with considering control factors.

Experiments were carried out on the constructed test rig. For each experimental run, the thin-walled part deformation, average surface roughness in the feed direction and transverse direction was measured respectively. Surface roughness was measured using an Olympus laser confocal microscope as shown in Fig. 2. The final values of R_a-*Fd* and R_a-*Td* under each experiment were calculated by the mean of 5 locations in the feed direction and transverse direction, respectively. The machining deformations of the thin-walled parts were detected using the global status three coordinate measuring machine (CMM) as shown in Fig. 3.

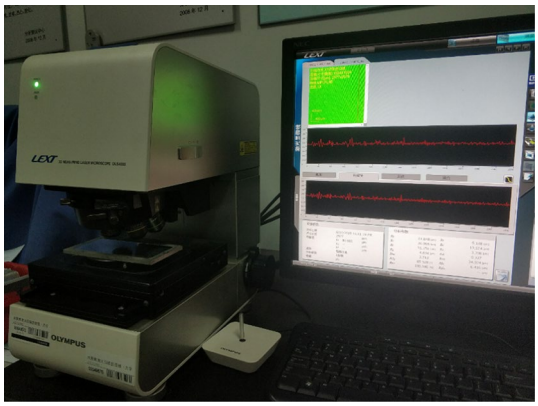

Fig. 2 Olympus laser confocal microscope

Fig. 3 Global status three-coordinate measuring machine

In this study, following the measuring method of thin-walled plate deformation proposed from Refs. [40–42], the machining deformation values of workpiece are measured along two directions (length direction and width direction) in response to before milling and after milling respectively. The position of the measured points on the top wall is shown in Fig. 4a. Before milling, a measuring point on fixture surface is set as basis point and its deformation is set to zero. Then, the CMM is used to measure the deformation variation by moving along two directions for the unmachined surface and record the data. After machining, the deformation measuring process is repeated on the finished surface, and the measurement points are arranged as the same with the unmachined surface. The deformation of each measured point is obtained by the difference of deformation values between unmachined surface and finished surface. According to Ref. [43], the maximum value of the measured deformation is suggested to develop the response model. Therefore, the obtained maximum deformation value is used in this study. The deformation measuring process for thin-walled plate is shown in Fig. 4.

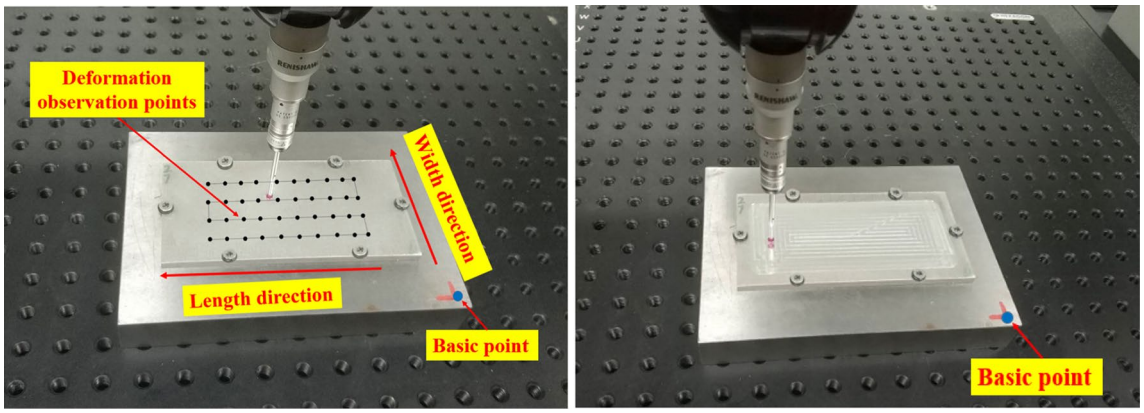

Fig. 4 Deformation measuring process for thin-walled plate **a** unmachined surface, **b** finished surface

3 Design of Experiments

In this paper, the primary objective of the experimental investigation is to analyze the influence of machining parameters on machining deformation and surface quality simultaneously. The selection of machining parameters in milling Al alloy thin-walled plates affects deformation, quality, and productivity of the machined parts [22]. Various parameters influence on surface roughness and machining deformation are investigated according to Refs. [6, 22, 41–43]. Among the machining parameters, the following control factors have the significant effect on surface roughness and machining deformation that are selected for evaluation in this paper: spindle speed, feed rate, transverse size, and depth of cut. The levels adopted for the control factors were defined considering tool supplier recommendations. The influences of spindle speed, feed rate, depth of cut, and transverse size were studied in terms of R_a-*Fd*, R_a-*Td*, and *TWD*. In order to test the effect of parameters on the three indicators, the RSM was used. The relationships between the parameters and responses are given as follows:

$$R_a - Fd = f(S, f, ts, doc) \tag{1}$$

$$R_a - Td = f(S, f, ts, doc) \tag{2}$$

$$TWD = f(S, f, ts, doc) \tag{3}$$

where R_a-*Fd,* R_a-*Td*, and *TWD* are the functions of the spindle speed, feed rate, transverse size, and depth of cut. In RSM, optimal design method is commonly used to construct the curvature of the model, which consisting of categorical factors and constrained regions. In addition, the evaluation of performance of developed model is analyzed by ANOVA, which helps to find out the significance of cutting parameters on the R_a-*Fd,* R_a-*Td*, and *TWD* respectively.

In this study, the analysis was performed using the Design Expert 8 software. All experimental runs were based on optimal design method that contains a total of 25 experimental runs. Four parameters (*S*, *f*, *ts*, *doc*) were selected as input variables to measure the R_a-*Fd,* R_a-*Td*, and *TWD* values as output results. 25 experiments were carried out and examined at various parametric conditions as list in Table 3.

4 Results and Discussion

In this study, for each experimental run, the R_a-*Fd,* R_a-*Td*, and *TWD* were measured respectively. Table 3 provides the measured R_a-*Fd,* R_a-*Td*, and *TWD* results in response to the various parametric factors. In RSM, the residual analysis was applied to check the adequacy of the proposed R_a-*Fd,* R_a-*Td*, and *TWD* models. In addition, ANOVA was applied to analyze the significance of cutting parameters on the R_a-*Fd,* R_a-*Td*, and *TWD* respectively. In the analysis, the associated p value of less than 0.05 indicates that the cutting parameters and their interactions are statistically significant.

4.1 Analysis of Surface Roughness in Feed Direction

Figure 5 shows two sample results of surface roughness at different parametric factors. It can be noticed that the cutting parametric factor influences the R_a-*Fd*. The normal plot of residuals and residuals versus run number for the R_a-*Fd* are shown in Fig. 6. For residual normal plot results, it can be observed that the points are closeness (close) to the straight line. In addition, there is no special pattern and unused structure in residuals versus run number. The above results conclude the proposed model adequacy.

According to Table 4, ANOVA results show that the spindle speed, feed rate, depth of cut and transverse size are the most significant factors on R_a-*Fd*. In addition, the most significant interaction factor is the depth of cut-transverse size

Table 3 Plan of experiments and their responses

Run no	Cutting factors				Responses		
	S (rpm)	*doc* (mm)	*ts* (mm)	*F* (mm/min)	R_a-*Fd* (μm)	R_a-*Td* (μm)	*TWD* (mm)
1	12,431	0.21	4.00	3600	4.583	3.952	0.060
2	14,490	0.22	5.26	6668	5.457	4.742	0.066
3	15,000	0.30	7.00	9000	6.540	4.979	0.105
4	12,840	0.10	4.96	9000	5.716	5.169	0.059
5	11,935	0.15	3.00	8892	5.394	5.527	0.060
6	12,780	0.30	3.00	6192	5.356	5.275	0.100
7	9000	0.10	3.00	8055	5.174	5.432	0.064
8	9000	0.30	3.00	9000	5.833	6.264	0.084
9	9000	0.22	5.44	6867	6.019	5.173	0.061
10	15,000	0.10	3.00	3600	4.263	4.028	0.051
11	9000	0.30	7.00	3600	5.594	4.028	0.079
12	9000	0.10	7.00	9000	5.987	5.394	0.086
13	12,810	0.20	7.00	3600	5.262	3.844	0.069
14	14,490	0.22	5.26	6668	5.591	4.825	0.052
15	11,400	0.10	4.34	5652	5.055	4.640	0.056
16	12,000	0.20	6.92	8783	6.056	5.053	0.071
17	11,400	0.10	4.34	5652	5.081	4.372	0.077
18	9000	0.26	3.00	3600	4.495	4.353	0.070
19	15,000	0.20	3.00	9000	5.290	5.179	0.055
20	15,000	0.10	7.00	6354	5.510	4.038	0.052
21	12,840	0.10	4.96	9000	5.386	5.005	0.062
22	12,780	0.30	3.00	6192	4.885	4.788	0.106
23	15,000	0.30	5.08	3600	4.864	3.854	0.105
24	9000	0.10	6.26	3600	4.653	3.918	0.067
25	9000	0.22	5.44	6867	5.764	5.044	0.066

interaction. Optimal design method containing 25 experimental runs was applied to establish the statistical model. According to the actual variables, the RSM model of surface roughness R_a-*Fd* is given by:

$$R_a - Fd = 2.68319 - 0.00003S - 0.360952doc + 0.088515ts + 0.000511f + 0.558146doc \cdot ts - 2.49357 \times 10^{-8} f^2 \quad (4)$$

The statistical model with R^2 and R^2_{adj} are list in Table 4. R^2 shows that the error of the regression model as a percentage of the total error (the multivariate correlation coefficient) is 94.72%, and the adjusted error as a percentage of the total error R^2_{adj} (that is, the modified multivariate correlation coefficient) is 92.96%, which is less than R^2.Also, the values of R^2 and R^2_{adj} are both greater than 85%.

The main effect represents direct the influence of cutting parameters on response variable. Figure 7 plots the main effect plot for R_a-*Fd*. It can be noted that the R_a-*Fd* correlates negatively with spindle speed. At low spindle speed, the built up edge (BUE) is formed and the chip fracture readily producing the rough surface. As the spindle speed increases, the BUE vanishes and chip fracture decreases, hence the surface roughness decreases [44, 45]. Thereby, a higher spindle speed leads to a smaller R_a-*Fd*.

The R_a-*Fd* almost linearly increases as the depth of cut and transverse size increase. This is because the cutting area and the cutting force increase with the increasing of the depth of cut and transverse size. Application of large and intermittent cutting forces during milling of low rigidity components results in regular deflections of thin wall during the machining operation. This causes the material removal in an uneven fashion and poor surface quality [6]. Therefore, a larger depth of cut or transverse size will lead to a larger surface roughness.

In addition, a non-linear increase of R_a-*Fd* with increasing of feed rate is observed. This is attributed to a higher feed rate leads to a higher cutting force and cutting heat temperature in the machining zone, thus cut chips deposit onto the work surface which results in poor surface quality [6, 45]. Hence, a high feed rate result in a large R_a-*Fd*. From

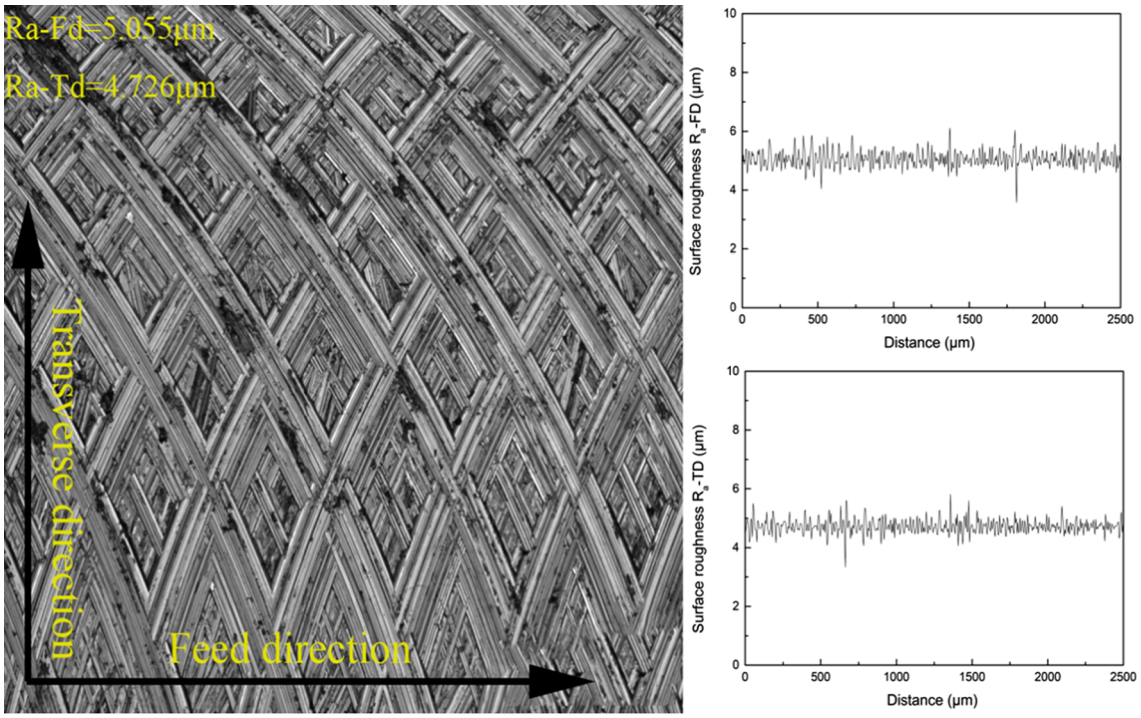

(a) *S*=11400 *rpm*, *doc*=0.1 *mm*, *ts*=4.34 *mm*, *f*=5652 *mm/min*.

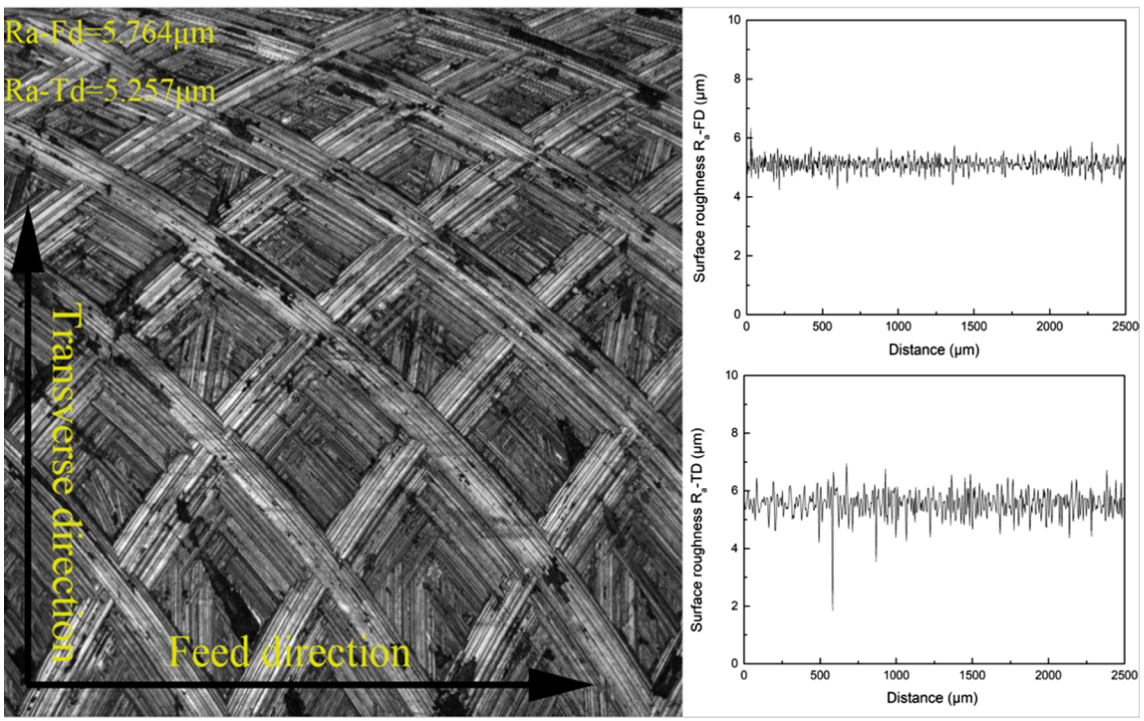

(b) *S*=9000 *rpm*, *doc*=0.22 *mm*, *ts*=5.44 *mm*, *f*=6867 *mm/min*.

Fig. 5 Measured surface roughness for different cutting parameters

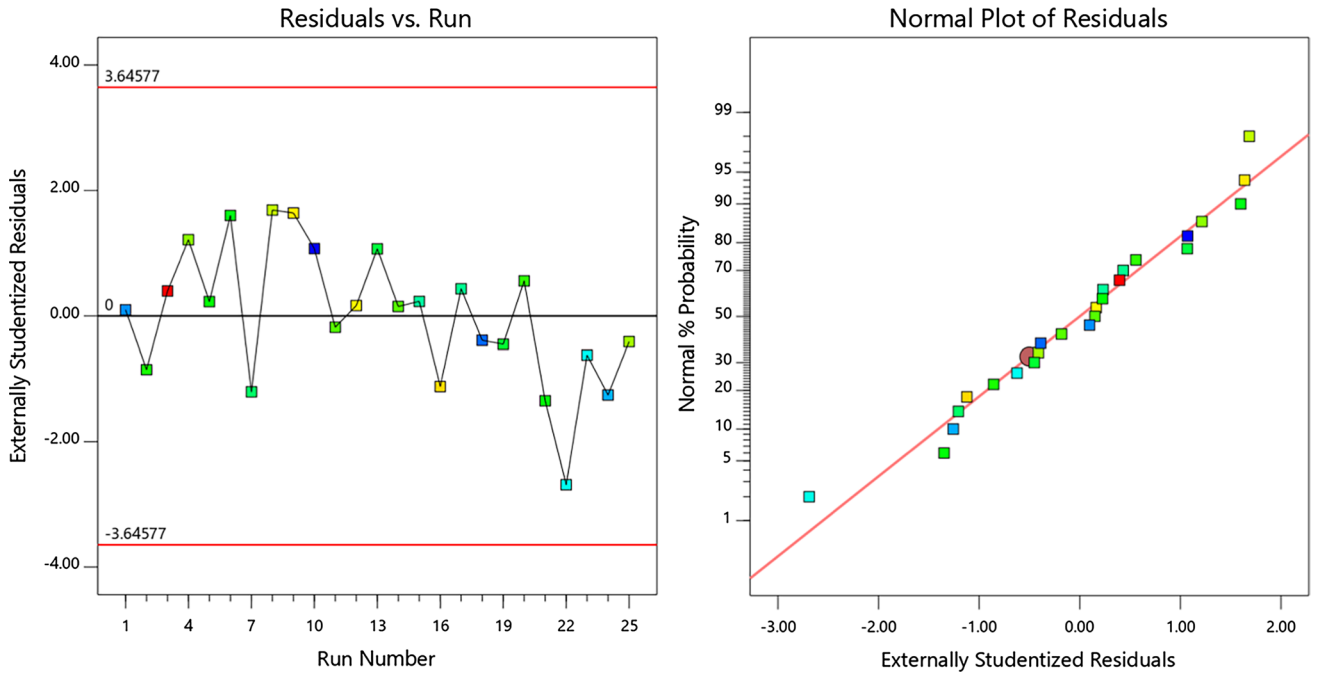

Fig. 6 Residual plot for surface roughness in feed direction

Table 4 Modified ANOVA results for surface roughness in feed direction

Source	Sum of squares	Degree of freedom	Mean of squares	*F*-value	*P*-value
Model	6.73	1	1.12	53.84	< 0.0001
S	0.1175	1	0.1175	5.64	0.0289
doc	0.8759	1	0.8759	42.05	< 0.0001
ts	2.33	1	2.33	111.99	< 0.0001
f	4.23	1	4.23	202.86	< 0.0001
doc·ts	0.1183	1	0.1183	5.68	0.0284
f^2	0.1658	1	0.1658	7.96	0.0113
Lack of fit	0.1675	13	0.0129	0.3107	0.9585
$R^2 = 0.9472$, $R^2_{adj} = 0.9296$					

above results, it is observed that a smaller R_a-*Fd* can be achieved by increasing the spindle speed or decreasing the feed rate, depth of cut, and transverse size.

4.2 Analysis of Surface Roughness in Transverse Direction

It can be also noticed from Fig. 5 that the cutting parametric factor influences the R_a-*Td*. Figure 8 shows the normal plot of residuals and residuals versus run number for the R_a-*Td*. Residual normal plot results shows the points are closeness to the straight line. Furthermore, no special pattern and unused structure is observed in residuals versus run number.

Table 5 presents ANOVA results for the R_a-*Td*. It is observed that the spindle speed, feed rate, transverse size, and depth of cut are the most significant factors on R_a-*Td*. In addition, interactions affecting the R_a-*Td* are: the most significant is spindle speed-feed rate interaction followed by depth of cut-feed rate interaction.

According to the actual variables, the RSM model of R_a-*Td* is given by:

$$\begin{aligned} Td = {} & 3.34602 + 0.000024S - 0.268298doc \\ & - 0.102436ts + 0.000402f \\ & - 1.66911 \times 10^{-8} Sf + 0.000299doc \cdot f \end{aligned} \quad (5)$$

The statistical model with R^2 and R^2_{adj} are list in Table 5. R^2 shows that the error of the regression model as a percentage of the total error is 96.49%, and the adjusted error as a

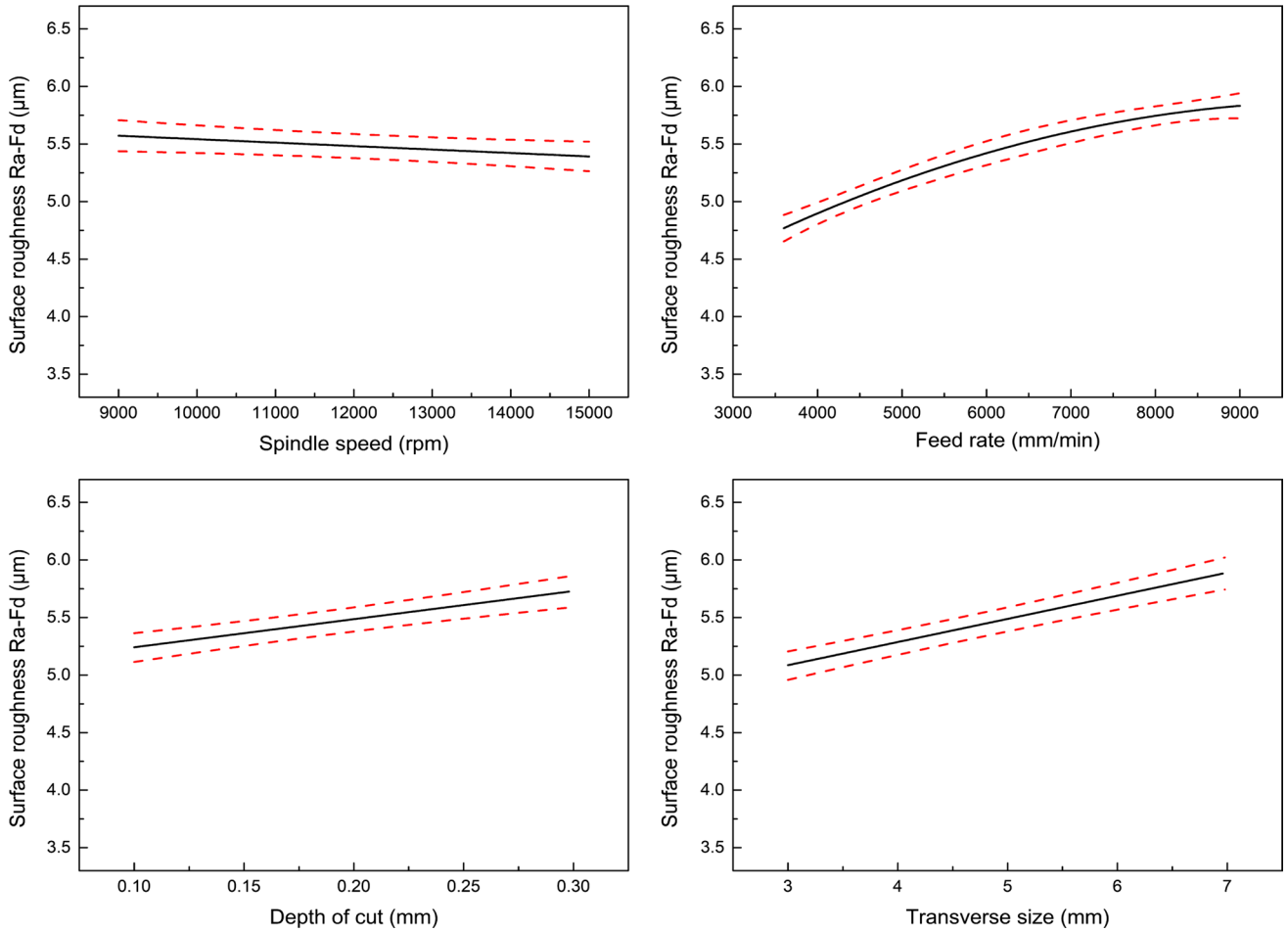

Fig. 7 Main effect plot for surface roughness in feed direction

percentage of the total error R^2_{adj} is 95.32%, which is less than R^2.Also, the values of R^2 and R^2_{adj}. are both greater than 85%.

The main effect plot for R_a-*Td* is shown in Fig. 9. As seen from Fig. 9, the R_a-*Td* decreases with increasing of the spindle speed, meanwhile, the R_a-*Td* increases as the feed rate and depth of cut increase. The explanations for these phenomena are already described in Sec. 4.1. For the transverse size, it found that the R_a-*Td* presents descending trend as transverse size increases. The observed trend is consistent with the pattern reported by other researchers [36, 37]. From above results, we reach the conclusion that a smaller R_a-*Td* can be obtained by increasing the spindle speed and transverse size or reducing the depth of cut and feed rate.

4.3 Analysis of Thin-Walled Part Deformation

Figure 10 shows the normal plot of residuals and residuals versus run number for the *TWD*. Residual normal plot results shows the points are closeness to the straight line. Furthermore, no special pattern and unused structure is observed in residuals versus run number.

Table 6 presents ANOVA results for the *TWD*. As shown in Table 6, the depth of cut is the most significant factors on the *TWD*. In addition, interactions affecting the *TWD* are: the most significant is spindle speed- depth of cut interaction followed by spindle speed -feed rate interaction.

The RSM model of *TWD* in terms of actual variables is given by:

$$\begin{aligned} TWD = {} & 0.04095 + 0.000013S - 0.990185doc \\ & + 0.001619ts + 5.70469 \times 10^{-6} f \\ & + 0.000034S \cdot doc - 4.42882 \times 10^{-10} S \cdot f \\ & - 7.41009 \times 10^{-10} S^2 + 1.89589doc^2 \end{aligned} \quad (6)$$

The statistical model with R^2 and R^2_{adj} are list in Table 6. R^2 shows that the error of the regression model as a percentage of the total error is 90.78%, and the adjusted error as a percentage of the total error R^2_{adj} is 86.17%, which is

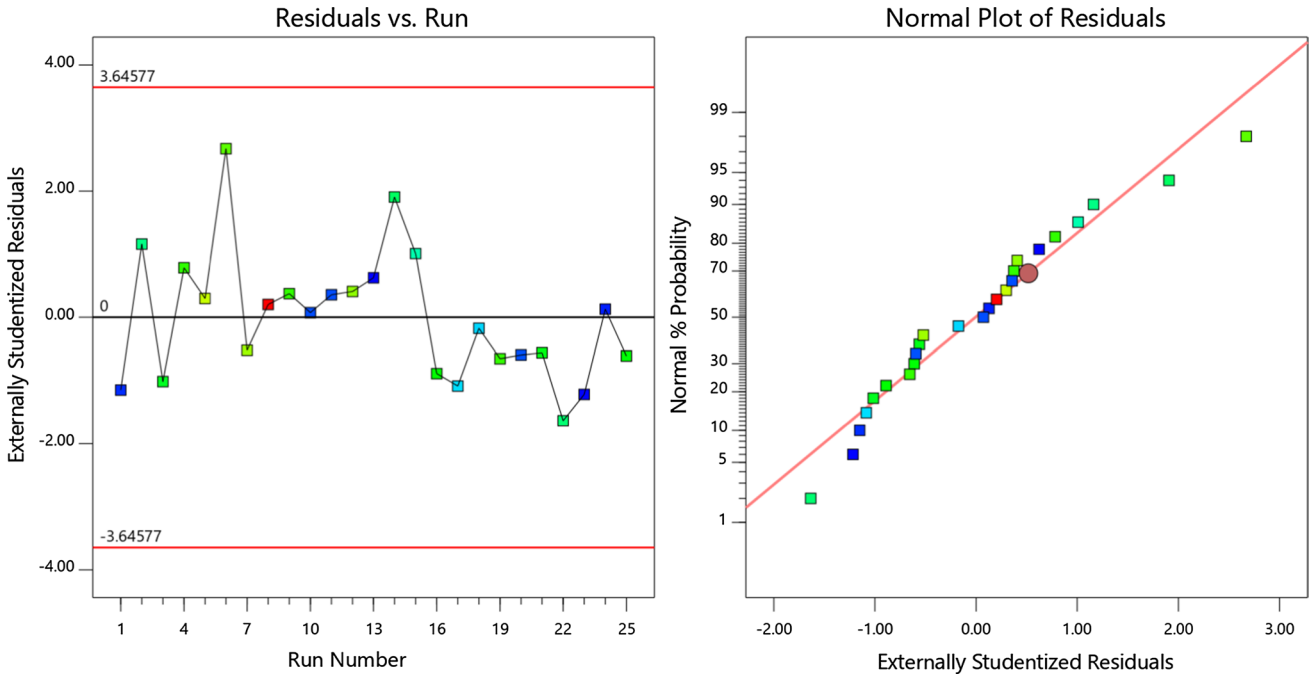

Fig. 8 Residual plot for surface roughness in transverse direction

Table 5 Modified ANOVA results for surface roughness in transverse direction

Source	Sum of squares	Degree of freedom	Mean of squares	*F*-value	*P*-value
Model	9.37	6	1.56	82.39	< 0.0001
S	0.8698	1	0.8698	45.90	< 0.0001
doc	0.3878	1	0.3878	20.47	0.0003
ts	0.5925	1	0.5925	31.27	< 0.0001
f	7.42	1	7.42	391.77	< 0.0001
$S \cdot f$	0.1697	1	0.1697	8.95	0.0078
$doc \cdot f$	0.0629	1	0.0629	3.32	0.0851
Lack of fit	0.1617	13	0.0124	0.3468	0.9425
$R^2 = 0.9649$, $R^2_{adj} = 0.9532$					

less than R^2.Also, the values of R^2 and R^2_{adj} are both greater than 85%.

Figure 11 shows the main effect plot for *TWD*. For the spindle speed, when the spindle speed reaches 11,653 rpm, the *TWD* increases up to 0.065 mm, after that, it starts to decrease as the spindle speed future increases. This is due to the residual stress of cutting and the cutting force increase with increasing of the spindle speed, which results in a larger deformation of thin-walled parts. However, when the spindle speed exceeds 11,653 rpm, the machining vibration tends to be stable as the cutting force and friction force decrease, hence the *TWD* decreases with increasing of the spindle speed.

In case of depth of cut, when the depth of cut reaches 0.151 mm, the *TWD* decreases up to 0.061 mm, and then, it starts to increase as the depth of cut increases rapidly. This is due to the involvement of the cutter in the cutting process becomes larger as the depth of cut increase, which cancels out a significant vibration of the workpiece, thus, the milling process become more stable, and the *TWD* becomes smaller. While the depth of cut increases, the removal material volume and the tool vibration increases, which leads to the *TWD* increases rapidly. Furthermore, the *TWD* is found to be increasing as the feed rate and transverse size increase, which is due to the increasing in

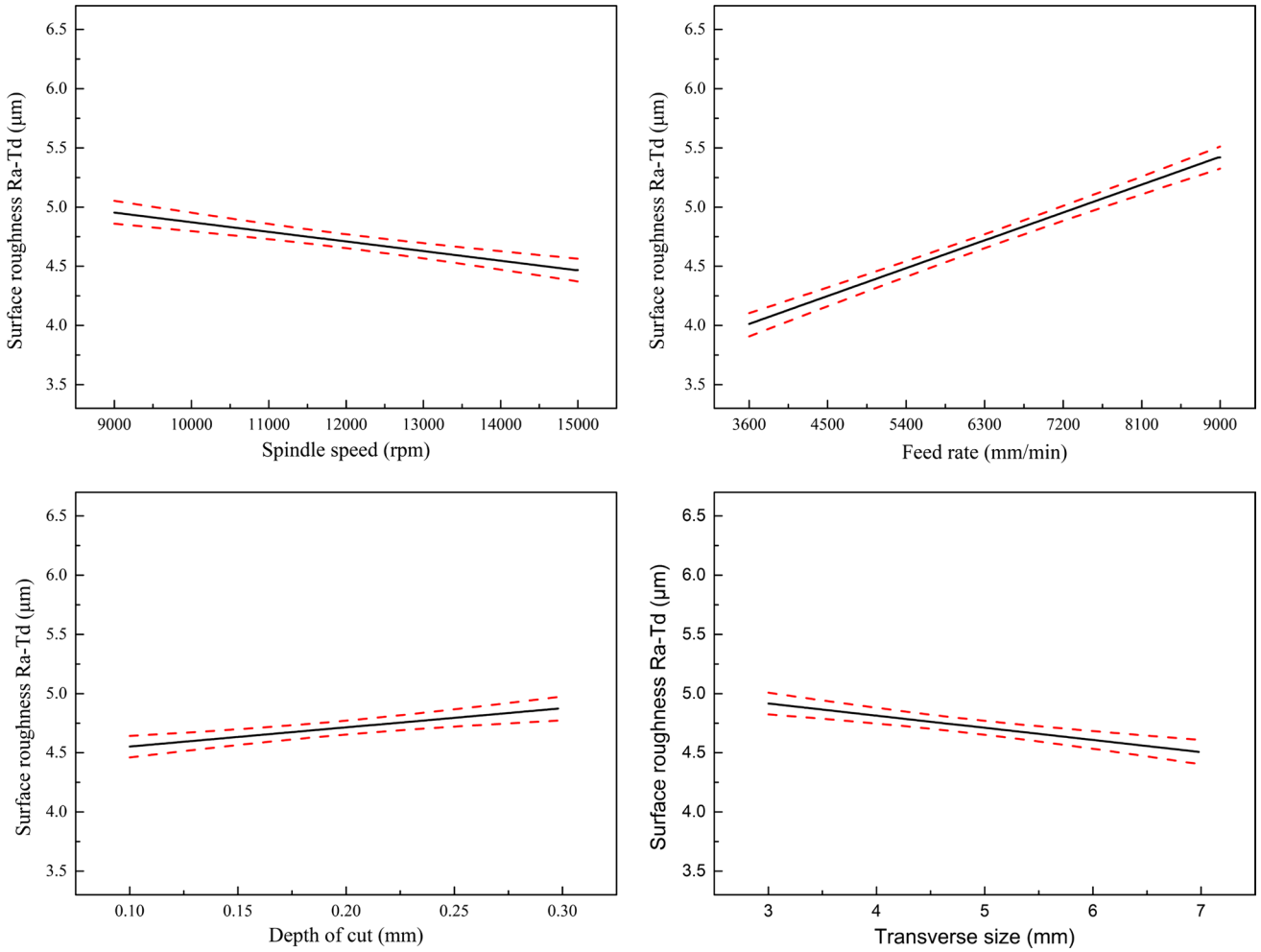

Fig. 9 Main effect plot for surface roughness in transverse direction

feed rate or transverse size makes the cutting force and the temperature between tool and chip thickness become higher, thus a higher feed rate or transverse size will result in a higher *TWD*.

From above analysis, it can be concluded that the R_a-*Fd*, R_a-*Td* are mainly influenced by the spindle speed, feed rate, transverse size and depth of cut, while the *TWD* is mainly influenced by the depth of cut. Thereby, we reach the conclusion that the depth of cut is the significant effect on the R_a-*Fd*, R_a-*Td*, and *TWD* simultaneously.

5 Results of Multi-objective Optimization

5.1 RSM-Optimum Function

This study aims to minimize the amplitude of deformation of thin-walled part and at same time minimize the surface roughness in feed direction and transverse direction. Moreover, the response parameters (R_a-*Fd*, R_a-*Td*, and *TWD*) are nonlinear multi-objective optimization problem due to the non-linear relationship between surface roughness, thin-wall part deformation and cutting parameters. The objective function is defined as follows:

$$\text{Minisize } (R_a - Fd, R_a - Td, TWD) \tag{7}$$

The constraints on the cutting parameters are as follows:

$$9000\,\text{rpm} \le S \le 15000\,\text{rpm}$$

$$3\,\text{mm} \le ts \le 7\,\text{mm}$$

$$3600\,\text{mm/min} \le f \le 9000\,\text{mm/min}$$

$$0.1\,\text{mm} \le doc \le 0.3\,\text{mm}$$

The optimal machining parameter predicted by RSM optimization functions are spindle speed 14,994 rpm, feed rate 3600 mm/min, transverse size 3.8 mm, and depth of

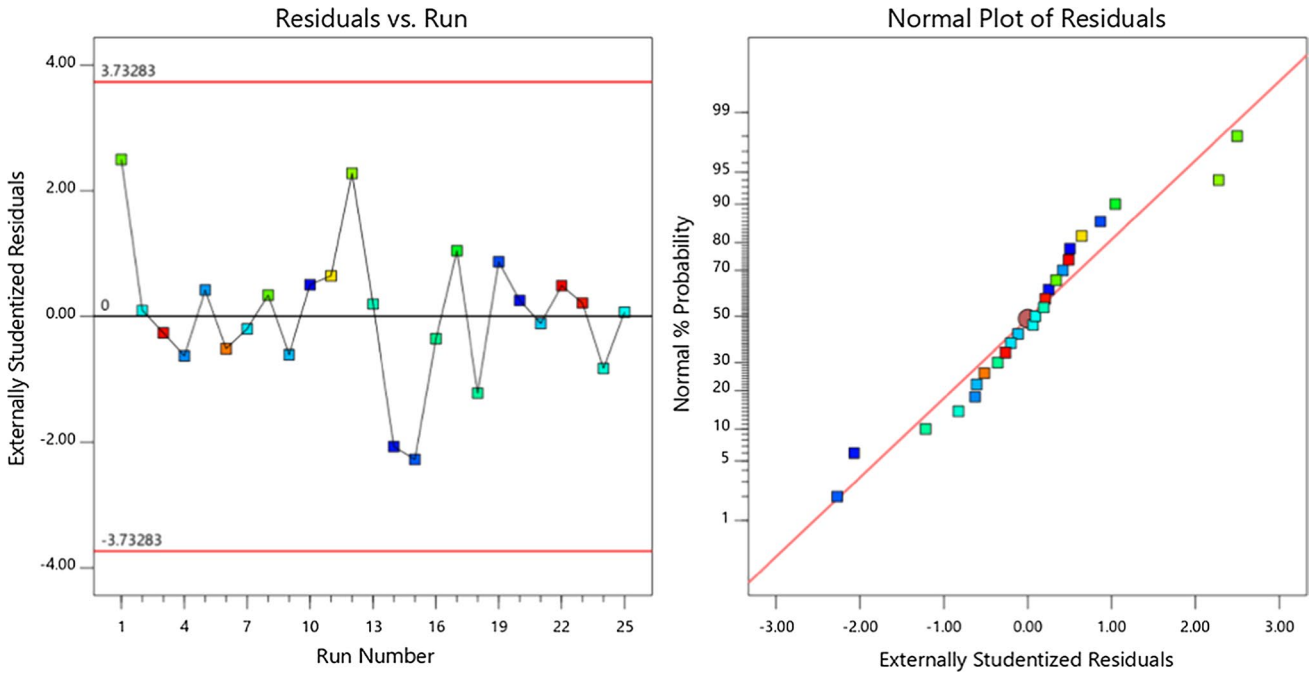

Fig. 10 Residual plot for thin-wall parts deformation

Table 6 Modified ANOVA results for thin-walled part deformation

Source	Sum of squares	Degree of freedom	Mean of squares	*F*-value	*P*-value
Model	0.0065	8	0.0008	19.69	< 0.0001
S	0.0000	1	0.0000	0.4035	0.5343
doc	0.0043	1	0.0043	103.65	< 0.0001
ts	0.0001	1	0.0001	3.41	0.0833
f	0.0000	1	0.0000	0.3972	0.5347
$S \cdot doc$	0.0010	1	0.0010	23.67	0.0002
$S \cdot f$	0.0001	1	0.0001	2.88	0.1092
S^2	0.0002	1	0.0002	4.98	0.0403
doc^2	0.0018	1	0.0018	42.76	< 0.0001
Lack of fit	0.0003	11	0.0000	0.4197	0.8931
$R^2 = 0.9078$, $R^2_{adj} = 0.8617$					

cut 0.1 mm. Meanwhile, the prediction results of R_a-*Fd,* R_a-*Td,* and *TWD* are 4.263 μm*,* 3.938 μm and 0.049 mm respectively, as list in Table 8.

5.2 ABC Algorithm Optimum

In this study, the ABC was used to find a set of optimal cutting parameters to achieve the optimal surface quality, that is, R_a-*Fd*, R_a-*Td*, and *TWD* simultaneously reach minimum values under a combination of optimal spindle speed, feed rate, depth of cut and transverse size. The ABC is a widely used meta-heuristic tool for multi-objective optimization with the advantages such as few control parameters, easy to implement, simple calculation, and it has a faster rate of convergence. Therefore, ABC algorithm is carried out to solve this multi-objective optimization problem by MATLAB programming. The optimization of cutting parameters by multi-objective ABC is obtained according to Fig. 12 as follows:

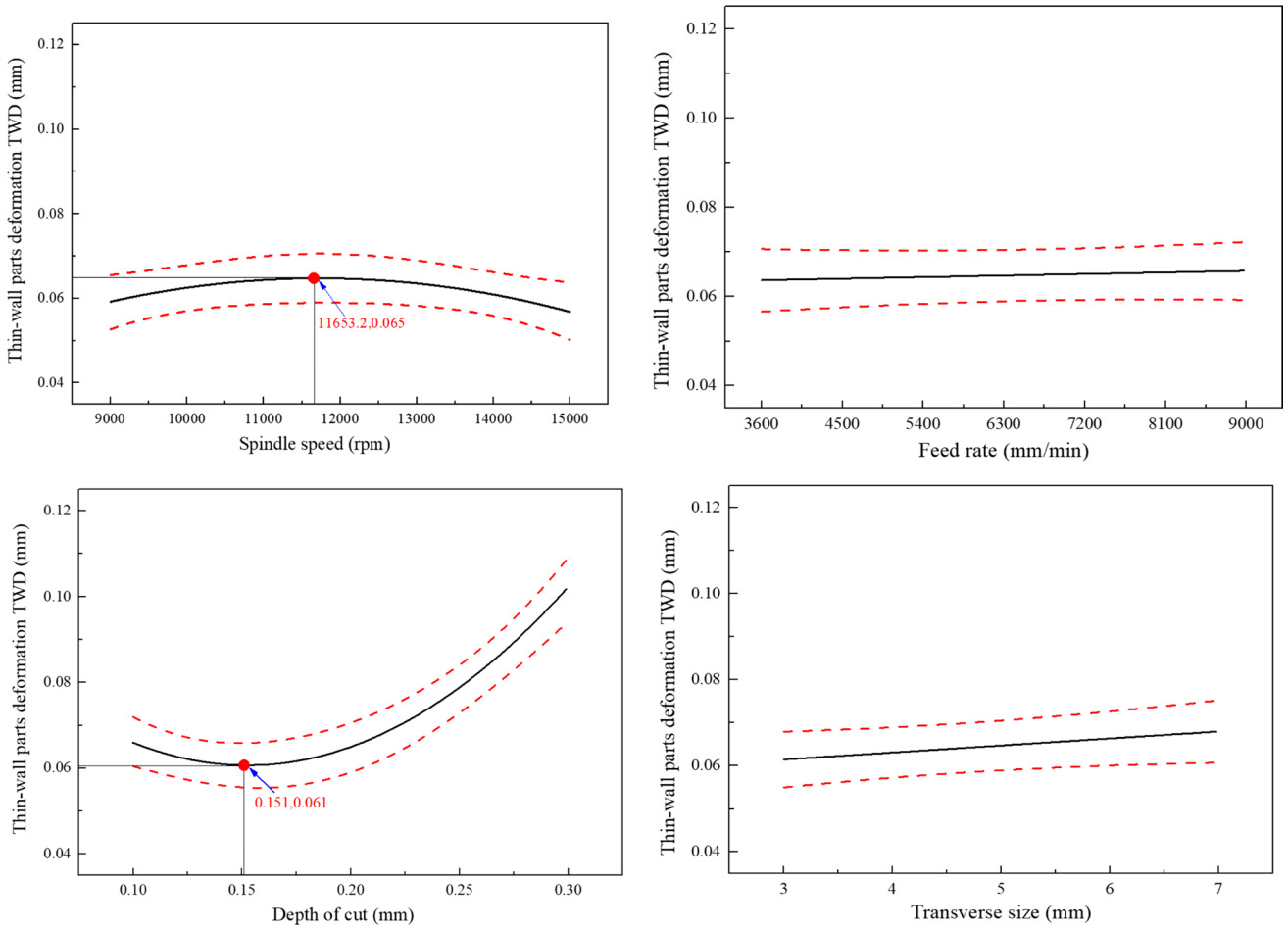

Fig. 11 Main effect plot for thin-wall parts deformation

Step 1 Initialize the parameters, both of the number of the employed bees and onlooker bees are set as 80. The maximum number of iterations are set as 500, and then, generate the food locations.

Step 2 The colonies are equally divided into 3 sub-colonies, and then, perform the select operation independently to each of the sub-objective functions in their individual sub-colonies.

Step 3 This is employed bee phase, where greedy selection is applied to select new food locations by calculating nectar amount for both of the original food locations and their neighborhood.

Step 4 In the onlooker bee phase, greedy selection is used to select new food locations after applying the roulette wheel selection to the results of the step 2.

Step 5 Determine if there is a solution to give up, if there is, then replace it with a randomly produced new location, or go straight to the next step.

Step 6 Memorize the best solution.

Step 7 The ABC continues to iterate until it reaches the maximum iteration number and finally outputs the optimal solution.

The convergence of the R_a-*Fd*, R_a-*Td*, and *TWD* are obtained after iteration as shown in Fig. 13. It can be seen that the R_a-*Fd*, R_a-*Td*, and *TWD* are continuously reduced via the continuous optimization of ABC. After convergence of the ABC, 15 best optimal points are obtained as the Pareto optimal points. The Pareto optimal solutions are listed in Table 7. In the actual machining process, to obtain the best surface quality, it is necessary to consider three responses (R_a-*Fd*, R_a-*Td*, and *TWD*) reach the smallest value stimulatingly. Therefore, the No.1 is considered as the optimal solution.

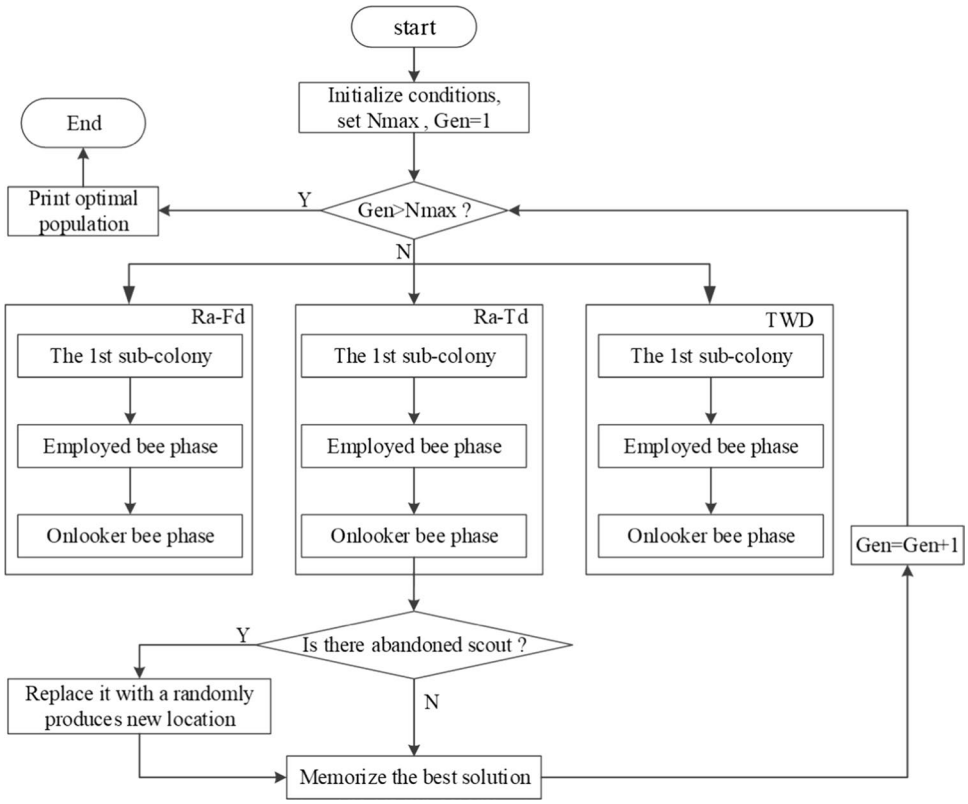

Fig. 12 Multi-objective ABC optimization flow chart

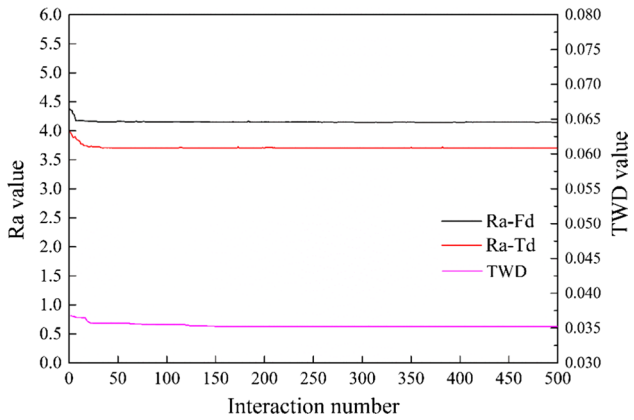

Fig. 13 The ABC optimum value of fitness

5.3 Comparison Between RSM And ABC Optimal Results

From above analysis, both RSM-optimum function and ABC algorithm can obtain the best values of R_a-*Fd*, R_a-*Td* and *TWD* respectively. Moreover, the RSM and ABC optimal results are compared as list in Table 8. Compared with RSM results, the values of R_a-*Fd*, R_a-*Td* and *TWD* obtained by ABC algorithm are improved by 2.7%, 2.2% and 16% respectively. Thereby, it can be concluded that the ABC algorithm can obtain a better cutting strategy.

Experiment was also conducted to validate the proposed cutting strategy. Comparison between prediction and experimental results are shown in Table 9. It can be seen that the prediction errors of the ABC algorithm optimum for the R_a-*Fd*, R_a-*Td* and *TWD* are 2.3%, 5.7% and 4.6% respectively.

6 Conclusions

In this paper, the influence of spindle speed, feed rate, depth of cut and transverse size on R_a-*Fd*, R_a-*Td* and *TWD* were investigated by milling of Al alloy 5083. Especially for the spindle speed and feed rate with a wider range were selected to increase the cutting efficiency. The R_a-*Fd*, R_a-*Td* and *TWD* prediction models were established by RSM, and the influence of cutting parameters on the R_a-*Fd*, R_a-*Td* and *TWD* were analyzed using ANOVA. For optimization process, a comparison of RSM-optimum function and artificial bee colony (ABC) algorithm optimum programming was performed to find the best cutting conditions leading to minimum R_a-*Fd*, R_a-*Td* and *TWD*

Table 7 Multi-objective solutions of ABC

No.	S (rpm)	doc (mm)	ts (mm)	f (mm/min)	$R_a - Fd$ (μm)	$R_a - Td$ (μm)	TWD (mm)
1	14,999.82	0.100063	3.000156	3601.123	4.1472	3.8509	0.0416
2	14,999.82	0.100039	3.000156	3601.123	4.1472	3.8509	0.0416
3	14,999.82	0.100063	3.000156	3601.123	4.1472	3.8509	0.0416
4	14,999.73	0.100039	3.000156	3601.123	4.1472	3.8509	0.0416
5	14,977.8	0.100132	6.998268	3601.102	4.7253	3.7007	0.0483
6	14,999.82	0.100059	3.007633	3601.123	4.1483	3.8515	0.0416
7	14,995.34	0.100039	6.993355	3601.118	4.7238	3.7001	0.0481
8	14,995.34	0.100039	6.993355	3601.118	4.7238	3.7001	0.0481
9	14,995.34	0.100039	3.006645	3641.065	4.1615	3.8577	0.0416
10	14,995.34	0.100039	6.993355	3601.118	4.7238	3.7001	0.0481
11	14,999.91	0.125164	3.002075	8997.142	5.2439	4.754	0.0352
12	14,999.91	0.135335	3.002167	8917.834	5.2522	4.7752	0.0355
13	14,999.91	0.127166	3.002075	8997.59	5.2466	4.7608	0.0352
14	14,999.95	0.125944	3.002102	8996.936	5.2449	4.7566	0.0352
15	14,999.95	0.127181	3.002075	8997.595	5.2466	4.7608	0.0352

Table 8 Comparison between RSM and ABC optimal results

	S (rpm)	doc (mm)	ts (mm)	f (mm/min)	$R_a - Fd$ (μm)	$R_a - Td$ (μm)	TWD (mm)	Improved		
								$R_a - Fd$	$R_a - Td$	TWD
RSM	14,994	0.10	3.80	3600	4.263	3.938	0.049	2.7	2.2	16
ABC	15,000	0.10	3.00	3601	4.147	3.851	0.041			

$$\text{Improved} = \frac{|ABC-RSM|}{RSM} \times 100\%$$

Table 9 Comparison between experimental and ABC optimal results

Responses	Exp. (μm)	ABC (μm)	Error (%)
R_a-Fd	4.053	4.147	2.3
R_a-Td	3.641	3.851	5.7
TWD	0.043	0.041	4.6

$$\text{Error} = \frac{|ABC-Exp.|}{Exp.} \times 100\%$$

simultaneously. According to analysis results, the following observations were drawn:

The response models are obtained for R_a-Fd, R_a-Td, and TWD in function of control factors. Three models present good data variability explanation with R^2 and R^2_{adj}, which proves the developed models are useful to study the process effects in the results.

ANOVA results show that the R_a-Fd, R_a-Td are mainly influenced by the spindle speed, feed rate, transverse size and depth of cut, while the TWD is mainly influenced by the depth of cut. Thereby, it can be concluded that the effect of depth of cut is much more pronounced than the effects of other factors on the R_a-Fd, R_a-Td, and TWD simultaneously.

Compared with traditional RSM optimization results, the ABC algorithm can obtain a better cutting strategy, and displays extensive favorable. The ABC algorithm optimum parameters are found to be spindle speed 15,000 rpm, depth of cut 0.1 mm, transverse size 3 mm, feed rate 3601 mm/min.

Confirmation experiment was performed to validate the proposed cutting strategy, the experimental results show a good coherence to the calculated results from ABC algorithm, which validates the performance of the proposed cutting strategy.

The RSM-ABC methodology used in this paper is detailed and can be applied in other manufacturing processes as a multi-objective modeling and optimization procedure. Moreover, the obtained results can be employed in the milling of Al alloy thin-walled parts, ensuring good surface roughness and low machining deformation.

Acknowledgements The authors are grateful to the National Defense Basic Research Fund Project of China (Grant No. A0720133010) for supporting this research.

References

1. Dejun, Y. A. N., Haiyang, L., Xiaoli, L., Meida, Z., Jiuqiang, L., & Zhimin, L. (2018). Microstructure and mechanical properties of variable polarity plasma arc welded joints of 5083 aluminum alloy for shipbuilding. *Rare Metal Materials and Engineering, 47*(10), 3161–3166.
2. Il, A., Chatelain, J.-F., Lalonde, J.-F., Balazinski, M., & Rimpault, X. (2018). An experimental investigation of the influence of cutting parameters on workpiece internal temperature during Al2024-T3 milling. *The International Journal of Advanced Manufacturing Technology, 97*(1–4), 413–426. https://doi.org/10.1007/s00170-018-1948-3.
3. Hao, Y., & Liu, Y. (2017). Analysis of milling surface roughness prediction for thin-walled parts with curved surface. *The International Journal of Advanced Manufacturing Technology, 93*(5), 2289–2297. https://doi.org/10.1007/s00170-017-0615-4.
4. Dikshit, M. K., Puri, A. B., & Maity, A. (2017). Modelling and application of response surface optimization to optimize cutting parameters for minimizing cutting forces and surface roughness in high-speed, ball-end milling of Al2014-T6. *Journal of the Brazilian Society of Mechanical Sciences and Engineering, 39*(12), 5117–5133. https://doi.org/10.1007/s40430-017-0865-y.
5. Li, J.-G., & Wang, S.-Q. (2017). Distortion caused by residual stresses in machining aeronautical aluminum alloy parts: recent advances. *The International Journal of Advanced Manufacturing Technology, 89*(1–4), 997–1012. https://doi.org/10.1007/s00170-016-9066-6.
6. Bolar, G., Das, A., & Joshi, S. N. (2018). Measurement and analysis of cutting force and product surface quality during end-milling of thin-wall components. *Measurement, 121*, 190–204. https://doi.org/10.1016/j.measurement.2018.02.015.
7. Qin, G., Wang, H., Lin, F., Sun, S., Guo, Y., Wu, T., et al. (2019). A new approach to deformation control of aeronautical monolithic components for aluminum alloy plates based on stress inverse and stress evaluation. *SCIENTIA SINICA Technologica*. https://doi.org/10.1360/SST-2019-0089.
8. Cagan, S. C., Venkatesh, B., & Buldum, B. B. (2020). Investigation of surface roughness and chip morphology of aluminum alloy in dry and minimum quantity lubrication machining. *Materials Today: Proceedings*. https://doi.org/10.1016/j.matpr.2020.01.547.
9. Vakondios, D., Kyratsis, P., Yaldiz, S., & Antoniadis, A. (2012). Influence of milling strategy on the surface roughness in ball end milling of the aluminum alloy Al7075-T6. *Measurement, 45*(6), 1480–1488. https://doi.org/10.1016/j.measurement.2012.03.001.
10. Wang, Z. H., Yuan, J. T., Liu, T. T., Huang, J., & Qiao, L. (2015). Study on surface roughness in high-speed milling of AlMn1Cu using factorial design and partial least square regression. *The International Journal of Advanced Manufacturing Technology, 76*(9), 1783–1792. https://doi.org/10.1007/s00170-014-6400-8.
11. Khanghah, S. P., Boozarpoor, M., Lotfi, M., & Teimouri, R. (2015). Optimization of micro-milling parameters regarding burr size minimization via RSM and simulated annealing algorithm. *Transactions of the Indian Institute of Metals, 68*(5), 897–910. https://doi.org/10.1007/s12666-015-0525-9.
12. Zeng, S., & Yuan, L. (2017). Optimization of milling process parameters based on real coded self-adaptive genetic algorithm and grey relation analysis. In Y. Huang, H. Wu, H. Liu, & Z. Yin (Eds.), *Intelligent Robotics and Applications* (pp. 867–876). Cham: Springer International Publishing. https://doi.org/10.1007/978-3-319-65298-6_77.
13. Vipindas, K., Kuriachen, B., & Mathew, J. (2019). Investigations into the effect of process parameters on surface roughness and burr formation during micro end milling of TI–6AL–4V. *The International Journal of Advanced Manufacturing Technology, 100*(5), 1207–1222. https://doi.org/10.1007/s00170-016-9210-3.
14. Sahu, N. K., & Andhare, A. B. (2017). Modelling and multiobjective optimization for productivity improvement in high speed milling of Ti–6Al–4V using RSM and GA. *Journal of the Brazilian Society of Mechanical Sciences and Engineering, 39*(12), 5069–5085. https://doi.org/10.1007/s40430-017-0804-y.
15. Pinar, A. M., Filiz, S., & Ünlü, B. S. (2016). A comparison of cooling methods in the pocket milling of AA5083-H36 alloy via Taguchi method. *The International Journal of Advanced Manufacturing Technology, 83*(9), 1431–1440. https://doi.org/10.1007/s00170-015-7666-1.
16. Karabulut, Ş., & Karakoç, H. (2017). Investigation of surface roughness in the milling of Al7075 and open-cell SiC foam composite and optimization of machining parameters. *Neural Computing and Applications, 28*(2), 313–327. https://doi.org/10.1007/s00521-015-2058-x.
17. Tlhabadira, I., Daniyan, I. A., Machaka, R., Machio, C., Masu, L., & VanStaden, L. R. (2019). Modelling and optimization of surface roughness during AISI P20 milling process using Taguchi method. *The International Journal of Advanced Manufacturing Technology, 102*(9), 3707–3718. https://doi.org/10.1007/s00170-019-03452-4.
18. Mahesh, G., Muthu, S., & Devadasan, S. R. (2015). Prediction of surface roughness of end milling operation using genetic algorithm. *The International Journal of Advanced Manufacturing Technology, 77*(1–4), 369–381. https://doi.org/10.1007/s00170-014-6425-z.
19. Zheng, K., Yao, J., & Dong, S. (2018). Surface roughness modeling and milling parameter optimization of 15–5PH stainless steel in milling arc surface. *Journal of the Brazilian Society of Mechanical Sciences and Engineering, 40*(4), 192. https://doi.org/10.1007/s40430-018-1127-3.
20. Lmalghan, R., Rao, K., ArunKumar, S., Rao, S. S., & Herbert, M. A. (2018). Machining parameters optimization of AA6061 using response surface methodology and particle swarm optimization. *International Journal of Precision Engineering and Manufacturing, 19*(5), 695–704. https://doi.org/10.1007/s12541-018-0083-2.
21. Chen, Y., Sun, Y., Lin, H., & Zhang, B. (2020). Prediction model of milling surface roughness based on genetic algorithms. In Z. Xu, K.-K. R. Choo, A. Dehghantanha, R. Parizi, & M. Hammoudeh (Eds.), *Cyber security intelligence and analytics* (pp. 1315–1320). Cham: Springer International Publishing. https://doi.org/10.1007/978-3-030-15235-2_179.
22. Qu, S., Zhao, J., & Wang, T. (2017). Experimental study and machining parameter optimization in milling thin-walled plates based on NSGA-II. *The International Journal of Advanced Manufacturing Technology, 89*(5), 2399–2409. https://doi.org/10.1007/s00170-016-9265-1.
23. Karkalos, N. E., Galanis, N. I., & Markopoulos, A. P. (2016). Surface roughness prediction for the milling of Ti–6Al–4V ELI alloy with the use of statistical and soft computing techniques. *Measurement, 90*, 25–35. https://doi.org/10.1016/j.measurement.2016.04.039.
24. Gao, Y.-Y., Ma, J.-W., Jia, Z.-Y., Wang, F.-J., Si, L.-K., & Song, D.-N. (2016). Tool path planning and machining deformation compensation in high-speed milling for difficult-to-machine material thin-walled parts with curved surface. *The International Journal of Advanced Manufacturing Technology, 84*(9), 1757–1767. https://doi.org/10.1007/s00170-015-7825-4.
25. Wang, J., Zhang, D., Wu, B., & Luo, M. (2018). Prediction of distortion induced by machining residual stresses in thin-walled components. *The International Journal of Advanced Manufacturing Technology, 95*(9), 4153–4162. https://doi.org/10.1007/s00170-017-1358-y.

26. Wu, Q., Li, D.-P., Ren, L., & Mo, S. (2016). Detecting milling deformation in 7075 aluminum alloy thin-walled plates using finite difference method. *The International Journal of Advanced Manufacturing Technology, 85*(5), 1291–1302. https://doi.org/10.1007/s00170-015-8012-3.
27. Yue, C., Chen, Z., Liang, S. Y., Gao, H., & Liu, X. (2019). Modeling machining errors for thin-walled parts according to chip thickness. *The International Journal of Advanced Manufacturing Technology, 103*(1), 91–100. https://doi.org/10.1007/s00170-019-03474-y.
28. Song, Q., Shi, J., Liu, Z., & Wan, Y. (2017). A time-space discretization method in milling stability prediction of thin-walled component. *The International Journal of Advanced Manufacturing Technology, 89*(9), 2675–2689. https://doi.org/10.1007/s00170-016-9379-5.
29. Jiang, X., Zhu, Y., Zhang, Z., Guo, M., & Ding, Z. (2018). Investigation of residual impact stress and its effects on the precision during milling of the thin-walled part. *The International Journal of Advanced Manufacturing Technology, 97*(1), 877–892. https://doi.org/10.1007/s00170-018-1941-x.
30. Jiang, X., Wang, Y., Ding, Z., & Li, H. (2017). An approach to predict the distortion of thin-walled parts affected by residual stress during the milling process. *The International Journal of Advanced Manufacturing Technology, 93*(9), 4203–4216. https://doi.org/10.1007/s00170-017-0811-2.
31. Guo, M., Jiang, X., Ye, Y., Ding, Z., & Zhang, Z. (2019). Investigation of redistribution mechanism of residual stress during multi-process milling of thin-walled parts. *The International Journal of Advanced Manufacturing Technology, 103*(1), 1459–1466. https://doi.org/10.1007/s00170-019-03640-2.
32. Cerutti, X., & Mocellin, K. (2016). Influence of the machining sequence on the residual stress redistribution and machining quality: analysis and improvement using numerical simulations. *The International Journal of Advanced Manufacturing Technology, 83*(1), 489–503. https://doi.org/10.1007/s00170-015-7521-4.
33. Li, B., Gao, H., Deng, H., Pan, H., & Wang, B. (2019). Investigation on the influence of the equivalent bending stiffness of the thin-walled parts on the machining deformation. *The International Journal of Advanced Manufacturing Technology, 101*(5), 1171–1182. https://doi.org/10.1007/s00170-018-2987-5.
34. Wimmer, S., Hunyadi, P., & Zaeh, M. F. (2019). A numerical approach for the prediction of static surface errors in the peripheral milling of thin-walled structures. *Production Engineering, 13*(3), 479–488. https://doi.org/10.1007/s11740-019-00901-7.
35. Wang, H., Zhou, M.-X., Zheng, W.-Z., Shi, Z.-B., & Li, H.-W. (2017). 3D machining allowance analysis method for the large thin-walled aerospace component. *International Journal of Precision Engineering and Manufacturing, 18*(3), 399–406. https://doi.org/10.1007/s12541-017-0048-x.
36. Yan, C. Q., Zhao, J., Li, Y. E., & Han, S. G. (2009). Experimental research on surface roughness in high speed milling of complex surface mold steel. In (Vol. 626, pp. 123–128): Trans Tech Publication. https://doi.org/10.4028/www.scientific.net/MSF.626-627.123.
37. Ren, W., Xu, J., Lin, J., Yu, Z., Yu, P., Lian, Z., et al. (2019). Research on homogenization and surface morphology of Ti-6Al-4V alloy by longitudinal-torsional coupled ultrasonic vibration ball-end milling. *The International Journal of Advanced Manufacturing Technology, 104*(1), 301–313. https://doi.org/10.1007/s00170-019-03668-4.
38. Arruda, É. M., de Paiva, A. P., Brandão, L. C., & Ferreira, J. R. (2019). Robust optimisation of surface roughness of AISI H13 hardened steel in the finishing milling using ball nose end mills. *Precision Engineering, 60*, 194–214. https://doi.org/10.1016/j.precisioneng.2019.07.013.
39. Zeroudi, N., & Fontaine, M. (2012). Prediction of machined surface geometry based on analytical modelling of ball-end milling. *Procedia CIRP, 1*, 108–113.
40. Gang, L. (2009). Study on deformation of titanium thin-walled part in milling process. *Journal of Materials Processing Technology, 209*(6), 2788–2793. https://doi.org/10.1016/j.jmatprotec.2008.06.029.
41. Ma, J.-W., Zhang, N., Chen, S.-Y., Su, W.-W., & Hu, G.-Q. (2018). Deformation analysing for thin-walled parts based on analysis of single-tooth or multi-tooth milling. *International Journal of Machining and Machinability of Materials, 20*(6), 575–593. https://doi.org/10.1504/IJMMM.2018.096383.
42. Wang, L.-Y., Huang, H.-H., West, R. W., Li, H.-J., & Du, J.-T. (2018). A model of deformation of thin-wall surface parts during milling machining process. *Journal of Central South University, 25*(5), 1107–1115. https://doi.org/10.1007/s11771-018-3810-z.
43. Han, Z., Jin, H., Fu, Y., & Fu, H. (2017). FEM numerical model and feedrate optimization based on-line deflection control of thin-walled parts in flank milling. *Journal of Mechanical Engineering, 2017*(21), 23. https://doi.org/10.3901/JME.2017.21.190.
44. Senthil, V., Kumar, S., & Raman, B. (2018). An integrated approach of RSM and MOGA for the prediction of temperature rise and surface roughness in the end milling of Al 6061-T6. *Transactions of FAMENA, 42*(3), 115–128. https://doi.org/10.21278/TOF.42308.
45. Bhushan, R. K., Kumar, S., & Das, S. (2010). Effect of machining parameters on surface roughness and tool wear for 7075 Al alloy SiC composite. *The International Journal of Advanced Manufacturing Technology, 50*(5), 459–469. https://doi.org/10.1007/s00170-010-2529-2.

Publisher's Note Springer Nature remains neutral with regard to jurisdictional claims in published maps and institutional affiliations.

De-Jun Cheng is a researcher of School of Mechanical Engineering at the Jiangsu University of Science and Technology. He received a BS in Mechanical Engineering from Jiangsu Ocean University in 2011 and an MS and PhD in Mechanical Engineering from Gyeongsang National University in 2013 and 2017, respectively. His research interests include tribology, heat and mass transfer and wear.

Feng Xu is a graduate student of School of Mechanical Engineering at the Jiangsu University of Science and Technology. He received a BS in Mechanical Engineering from Changshu Institute of Technology in 2017. His research interests include precision machining and green manufacturing.

Sheng-Wen Zhang is a professor and master advisor of Jiangsu University of Science and Technology. He received his Ph.D.degree in mechanical manufacturing in Jiangsu University in 2013. The main research directions are CAD/CAPP/CAM integration technology and Group Technology. His research interests also include advanced processing technology and equipment and digital manufacturing systems.

Sheng-Hao Xu is a graduate student of School of Mechanical Engineering at the Jiangsu University of Science and Technology. He received a BS in Mechanical Engineering from Yancheng Institute of Technology in 2019. His research interests include intelligence algorithm, numerical calculation, mechanics and mass transfer and wear.

Su-Jin Kim is a professor of Mechanical Engineering at the Gyeongsang National University. He reveived a BS in An Agricultural Mechanical Engineering from Seoul National University in 1998 and an MS and PhD in Mechanical Engineering from Korea Advanced Institute of Science and Technology in 2000 and 2005, respectively. His research interests include computer-aided manufacturing and NC machining simulation.

Chun-Yan Zhang is a researcher of School of Mechanical Engineering at the Jiangsu University of Science and Technology.She received a BS in Material Engineering of Kunming University of Science and Technology in 1998 and an MS in Environment Engineering from Jiangsu University in 2004 and PhD in Mechanical Engineering from Jiangsu University in 2008. Her research interests include precision machining and green manufacturing.